European Review for Medical and Pharmacological Sciences 2020; 24: 5714-5725

Experimental study on synergistic effect of HIFU treatment of tumors using *Bifidobacterium* bound with cationic phase-change nanoparticles

B.-L. JIANG[1,2], X. GAO[1], J. XIONG[1], P.-Y. ZHU[3], Y. LUO[1], D. XU[1], Y. TANG[1], Y.-T. WANG[1], C. CHEN[1], H.-Y. YANG[1], H. QIAO[1], J.-Z. ZOU[1]

[1]State Key Laboratory of Ultrasound Engineering in Medicine Co-Founded by Chongqing and the Ministry of Science and Technology, College of Biomedical Engineering, Chongqing Key Laboratory of Biomedical Engineering; Chongqing Medical University, Chongqing Collaborative Innovation Center for Minimally-Invasive and Noninvasive Medicine, Chongqing, China
[2]Sichuan Key Laboratory of Medical Imaging, North Sichuan Medical College, Nanchong, China
[3]Department of Clinical Medicine, North Sichuan Medical College, Nanchong, Sichuan, China

Abstract. – OBJECTIVE: Anaerobic bacteria can enter the solid tumor in the hypoxic region to colonize and proliferate. Aggregation of nanoparticles in the tumor area can enhance molecular imaging and therapy. It is hypothesized that the combination of the two could possibly achieve better imaging and tumor treatment. This study presents a biocompatible bacteria-based system that can deliver cationic phase-change nanoparticles (CPNs) into solid tumor to achieve enhanced imaging and treatment integration.

MATERIALS AND METHODS: Cationic phase-change nanoparticles (CPNs) and *Bifidobacterium longum* (BF) were mixed to determine the best binding rate and were placed in an agar phantom for ultrasonography. BF-CPNs complex adhesion to breast cancer cells was observed by laser confocal microscopy. *In vivo,* BF-CPNs and control groups were injected into tumors in breast cancer nude mouse models. Nanoparticles distribution was observed by ultrasound and *in vivo* fluorescence imaging. HIFU ablation was performed after injection. Gross and histological changes were compared and synergy was evaluated.

RESULTS: *Bifidobacterium longum* (BF) and CPNs were combined by electrostatic adsorption. The BF-CPNs particles could increase the deposition of energy after liquid-gas phase-change during High Intensity Focused Ultrasound (HIFU) irradiation of tumor.

CONCLUSIONS: This study shows a valid method in diagnosis and therapy integration for providing stronger imaging, longer retention time, and more effective tumor treatment.

Key Words:
Bifidobacterium longum, Cationic phase-change nanoparticles, HIFU, Treatment

Introduction

High-intensity focused ultrasound (HIFU) can concentrate ultrasonic energy on a targeted region. Its intrinsic focusing and tissue penetration support an exact tumor treatment[1,2]. However, HIFU application in larger tumor ablation has some disadvantages such as long treatment time, skin burns, and damage to surrounding normal tissues. Attempts have been made to improve safety and efficacy of HIFU treatment by optimizing the ultrasound irradiation parameters, changing the irradiation mode, and so on[3,4]. Ultrasound contrast microbubbles can synergistically work with HIFU as they have high acoustic impedance, cause cavitation, and undergo rupture. They enhance tumor imaging and help monitor ablation during the implementation of a therapeutic platform[5-8]. SonoVue synergist has been clinically proved to be effective in shortening treatment time and mitigating side effects[7,9-11]. However, micron-size diagnostic ultrasound microbubbles are too large to penetrate vascular endothelial space, and they have short half-life. Thus, as an ablation mediator for tumor treatment, it has been limited in practicality[12]. In comparison, nanoscale ultra-

Corresponding Author: Jianzhong Zou, MD; e-mail: zoujzh@cqmu.edu.cn

sound contrast agents have a good synergy and can penetrate the high permeable tumor blood vessel walls to reach into the interstitial spaces[13,14]. Recent advances in targeted nanoparticles (NPs) and acoustically activated microbubbles created many new opportunities for molecular targeting and image-guided therapy using clinical ultrasound[15-17]. Several researchers[12,14,18,19] have introduced liquid fluorocarbon-encapsulated NPs for HIFU synergist. Nevertheless, NPs are extremely small, and their imaging is based on aggregation. Echo signal resolution with nanobubbles is lower than that obtained by harmonic imaging with microbubble-enhanced ultrasound. Moreover, intravenous injection of the contrast agents in the tumor and surrounding tissues can damage adjacent normal organs. Therefore, we aimed to improve NPs aggregation in the tumor area, enhance ultrasound imaging, and adapt NPs to HIFU treatment.

Bifidocaterium longum (BF) is endemic probiotic bacteria in human and other mammalian intestines. It can proliferate in the hypoxic zones of tumors[20] and has been used for biological targeting in antitumor gene therapy[21,22]. BF is Gram-positive, and it has negative charges on its surfaces since its cell walls contain a lot of proteins. Thus, it is feasible to combine the positive charge of cationic phase-change nanoparticles (CPNs) with the negative charge of BF. In this study, BF and CPNs binding were assessed *in vitro* and *in vivo*, and their ultrasound imaging and synergy with HIFU were evaluated.

Materials and Methods

Chemicals

All chemicals were directly used without further purification. 1, 2-dioleoyl-sn-glycero-3-phosphocholine(DOPC), 3β-[N-(N',N'-dimethylaminoethane)-carbamoyl] cholesterol (DC-chol)1, 2-distearoyl-sn-glycero-3-phosphoethanolamine-N-[methoxy (polyethylene glycol 2000] ammonium salt (DSPE-PEG2000; Avanti Polar Lipids, Alabaster, AL, USA). Perfluorohexane (PFH; Apollo Scientific, Stockport, UK). Bifidobacterium longum ATCC-15707 (American Type Culture Collection, ATCC, Manassas, VA, USA). Human breast cancer cells MDA-MB-231 (Laboratory of Life Sciences School, Chongqing Medical University, Chongqing, China). 4', 6-diamidyl-2-phenylindole (DAPI), 1, 1'-octadecyl-3, 3, 3', 3'-tetramethylindocyanine iodide (DiR). Fluorescein isothiocyanate (FITC), 1, 1'-dioctadecyl-3, 3, 3', 3'-tetramethylindocarbocyanine-perchlorate DiI) (Sigma-Aldrich Corp., St. Louis, MO, USA).

Instruments

Malvern laser particle size detector (Malvern, UK). Flow cytometry (BD Bioscience, Franklin Lakes, NJ, USA). Caliper IVIS Lumina II (CRi Maestro; Cambridge Research & Instrumentation, Inc, Hopkinton, MA, USA). NikonA1R confocal microscope (Nikon Corporation, Tokyo, Japan). NanoDrop™ 2000 ultramicro spectrophotometer (Thermo Fisher Scientific, Waltham, MA, USA), HIFU JC-200 ultrasound therapeutic instrument (Haifu Company, Chongqing Medical University, Chongqing, China). Philips EPIQ7 ultrasound diagnostic instrument (Philips, Amsterdam, the Netherlands).

Preparation and Characterization of CPNs

CPNs were prepared by the film-ultrasonic technique[23]. Cationic lipid DC-cholesterol and neutral phospholipids (DPPC and DSPE-PEG2000) were dissolved at a 5:2:2 mass ratio in chloroform and methanol (2:1 v/v). The solution was spun in a rotary evaporator for 50 min to remove the organic solvents and leave a uniform lipid film at the bottom of the bottle. Then, 2 mL double-distilled water was added to the bottle and the mixture was shaken until hydration occurred. The resultant translucent suspension was placed in an ice water bath. One hundred microliters of PFH was dropwise added, and the mixture was emulsified for 10 min with an ultrasonic cell crusher at 150 W and a 5 s on /5 s off cycle. The NPs emulsion was centrifuged at 8,000 g and 4°C for 10 min in a hypothermic centrifuge. This process was repeated twice. To prepare fluorescent NPs, DiI or DiR was added to the solution, and then it was covered with silver papers in the dark to prevent light exposure. Subsequently, the same procedures were adopted as detailed above. The NPs were resuspended and stored at 4°C until later use. NPs size and zeta potential were measured by a Malvern particle size analyzer.

Culture and Characterization of BF

BF was cultured in MRS broth under anaerobic conditions at 37°C for 24 h. Bacteria were collected by centrifugation at 4°C and 6000 g for 5 min, diluted with phosphate-buffered saline

(PBS; pH 7.4), dyed with FITC, and stored in an ice water bath until later use. Particle size and zeta potential were measured in a Malvern particle size analyzer.

Optimum Binding Ratio of BF and CPNs

The CPNs and BF were diluted as described above. OD_{600} = 0.1 for both the CPNs and the BF. The density of the latter was 6.2×10^6 cfu/mL. BF and CPNs were mixed at 3:1, 5:1, 1:1, and 1:2. The suspensions were observed with the unaided eye and under a light microscope. Then, 1 mL each of the DiI-stained 3:1, 5:1 BF-CPNs suspensions and a negative BF control at the same concentration were evaluated by flow cytometry.

Ultrasound Observation of BF-CPNs Binding

A coagulated agar gel phantom was prepared with surface conical holes of equal diameter. The BF-CPNs mixture was added to the phantom and compared with degassed water and BF alone or CPNs alone. Two-dimensional ultrasound images of all suspensions were obtained with a linear-array ultrasonic probe at 8-12 MHz. Gray values were determined with a DFY ultrasonic imaging quantitative analyzer.

Observation of BF-CPNs Cellular Adhesion

Human breast cancer cells (MDA-MB-231) in log-phase were inoculated into confocal culture dishes and 100 μL DAPI (10 μg/mL) was added. The cells were incubated overnight. When all cells had adhered to the vessel wall, the culture medium and unreacted dye were removed. Then, 1 mL methanol was added, and the cells were incubated for 10 min. The methanol was removed and the cells were washed twice with PBS. FITC-labeled BF and DiI-labeled CPNs (OD_{600} = 0.1) were mixed at a 3:1 volumetric ratio. Then, 100 μL of this mixture was added to the cell culture dish and left to react for 10 min. Unreacted material was removed, and the cells were washed twice with PBS. Control culture dishes were simultaneously prepared by adding equal volumes of BF and NPs.

Animals and Model Establishment

This investigation was approved by the Animal Ethics Committee of Chongqing Medical University Animal Center. Female BALB/c nude mice aged 2-4 weeks and weighing 14-18 g (Animal Experimental Center of Chongqing Medical University, Chongqing, China) were placed in separate cages and fed a mixed diet. All animal experiments were performed in accordance with the guidelines of the National Institute of Health of the USA. Human breast cancer cell lines were cultured in Dulbecco's Modified Eagle's Medium (DMEM) with high sugar content (Gibco, Rockville, MD, USA) and 10% (w/v) fetal bovine serum (FBS; Gibco, Rockville, MD, USA). The cells were extracted at the log phase and washed thrice and resuspension with PBS. The cell density was adjusted to 10^8 mL^{-1}. An injection of 0.1 mL suspension was administered into the buttocks of healthy nude mice. When the tumor volume reached about 100 mm^3, the mice were sacrificed. The tumors were excised and blocks of 1 mm^3 were prepared from them. The buttock skin and subcutaneous tissue were separated to form a capsular bag in which the tumor was implanted. The incisions were closed with absorbable sutures. The mice were fed *ad libitum* and tumor growth was monitored. When the tumor diameter reached 1 cm at 2-3 weeks after formation, the next phase of the experiment was initiated.

Ultrasound-Guided Local Intratumoral BF-CPNs Injection

BF and CPNs were mixed at a 3:1 volumetric ratio. The optical density (OD_{600}) was set to 0.1 and 0.3, respectively, for the BF-CPNs1 and BF-CPNs2 experimental groups. OD_{600}=0.3 was set for the separate BF and CPNs which were used as controls. PBS was the blank control. 30 tumor-bearing nude mice were used, and there were 6 in each group. Linear array probes were used for ultrasound inspection. The operating parameters were 8-12 MHz, mechanical index 0.08, 2D mode, and contrast-enhanced real-time display mode. 15 μL of the prepared solution were injected by microsyringe into the tumor center on the buttock of each mouse. Ultrasonic images were recorded at 10 min, 30 min, 60 min, 90 min, 12 h, 24 h, and 48 h after injection. Changes in the mean local gray values in the injection areas were measured by a DFY ultrasound imaging quantitative analyzer.

In-Vivo Fluorescence Observation

At 1 h, 24 h, and 48 h after injection, the relative fluorescence intensities of the tumor areas in the CPNs and BF-CPNs2 groups were measured by a Caliper IVIS Lumina II system. The excitation and emission wavelengths were 748 nm and 780 nm, respectively.

BF Binding with CPNs Enhancement of the HIFU Effect

At 48 h after injection, each group was received the same power for systematic evaluation by HIFU irradiation experiments (acoustic power 150 W, irradiation duration 2 s). Changes in mean gray value and areas of the changes were measured before and after ablation. 24 h after HIFU treatment, the tumor tissues were dissected and one mouse was randomly selected per group for histological blood and tissue culture observations. Other tumors were stained with 2% TTC solution in 37°C for gross morphological observation.

General Observation and Measurement of Ablation Volume and Evaluation Standard

Tumors were longitudinally cut into 2 mm sections along the direction of incident irradiation and stained with TTC. Coagulation necrosis was observed by unaided eye. Ablated volumes were measured and calculated as follows: $V = \pi/6 \times \text{length} \times \text{width} \times \text{depth}$ (mm^3).

After HIFU treatment, the mice were sacrificed and the tumors were removed and were fixed with 4% (w/v) paraformaldehyde for 24 h, dehydrated, and embedded with paraffin. Paraffin sections 4 μm thick were prepared. Two sections per group were randomly selected for hematoxylin and eosin (H&E) staining and two others for Gram staining. All were observed under microscope.

Blood and Tissue Cultures

Nude mice were anesthetized and 0.5 mL blood was aspirated from their hearts. Heart, liver, spleen, lung, kidney, and tumor tissues were excised after scarification, weighed, homogenized, and passed through 100-mesh sieves. The samples were diluted with PBS to prepare a concentration gradient. 100 μL dilutions were cultured in solid BL medium for 72 h.

Statistical Analysis

Data were analyzed by Statistical Product and Service Solutions (SPSS) version 19.0 (IBM Corp., Armonk, NY, USA) and expressed as means ± standard deviation (SD). The SNK-q test was used to compare pairs of group means. $p<0.05$ indicated significant difference.

Results

Characterizations and In-Vitro Binding of BF-CPNs

The CPNs suspension was milky white. Optical microscopy revealed that it contained numerous refractive spherical NPs uniform in size and with good dispersion. The particle size and zeta potential were 314 ± 52.6 nm and 29.7 ± 7.6 mV, and remained constant after 1 week storage at 4°C. The BF diameter was 4,104 ± 547.3 nm and the zeta potential was -31.6 ± 5.8 mV. The zeta potential of the BF-CPNs mixture was -0.4 ± 2.9 mv (Figure 1A).

BF and CPNs suspensions mixed at various ratios were observed with the unaided eye. Flocculent precipitation was occurred in the tubes containing the 1:1 and 1:2 ratio BF and CPNs suspensions. Light microscopy revealed aggregation of large numbers of BF and NPs. The 3:1and 5:1ratio BF and CPNs suspensions did not precipitate after standing 10 min. Dispersed BF with NPs attached to their surfaces were observed under a light microscope (Figure 1B). Flow cytometry indicated that the binding rate of the BF and NPs was 99.6% in the 3:1 mixture (Figure 1C).

The 2D ultrasonography in gel mode showed poor images of pure BF or CPNs. On the other hand, varying degrees of echo contrast were obtained for the BF-CPNs mixtures. The gray values of the 3:1- and 5:1-ratio BF-CPNs mixtures were the highest measured (Figure 1D) and significantly differed from those for the blank control and separate BF and CPNs. At BF: CPNs= 3:1, the sonogram disclosed fine uniformly distributed light spots whose gray values were the highest. The gray value decreased with increasing CPNs proportion for the tubes containing 1:1 and 1:2 BF: CPNs. The gray scale images strongly revealed large reflective spots in the dark background. This observation was consistent with the nanoparticle and bacterial aggregation observed microscopically. The gray value of the 1:2 ratio BF: CPNs suspension was lower than that for the CPNs alone (Figure 1E).

CPNs Promoted BF Adhesion to Cells with a Double-Sided Adhesive Effect

When NPs alone were added to the cells, they accumulated around them (Figure 2A). In contrast, BF alone did not adhere to the cells (Figure 2B). When the BF-CPNs complex was

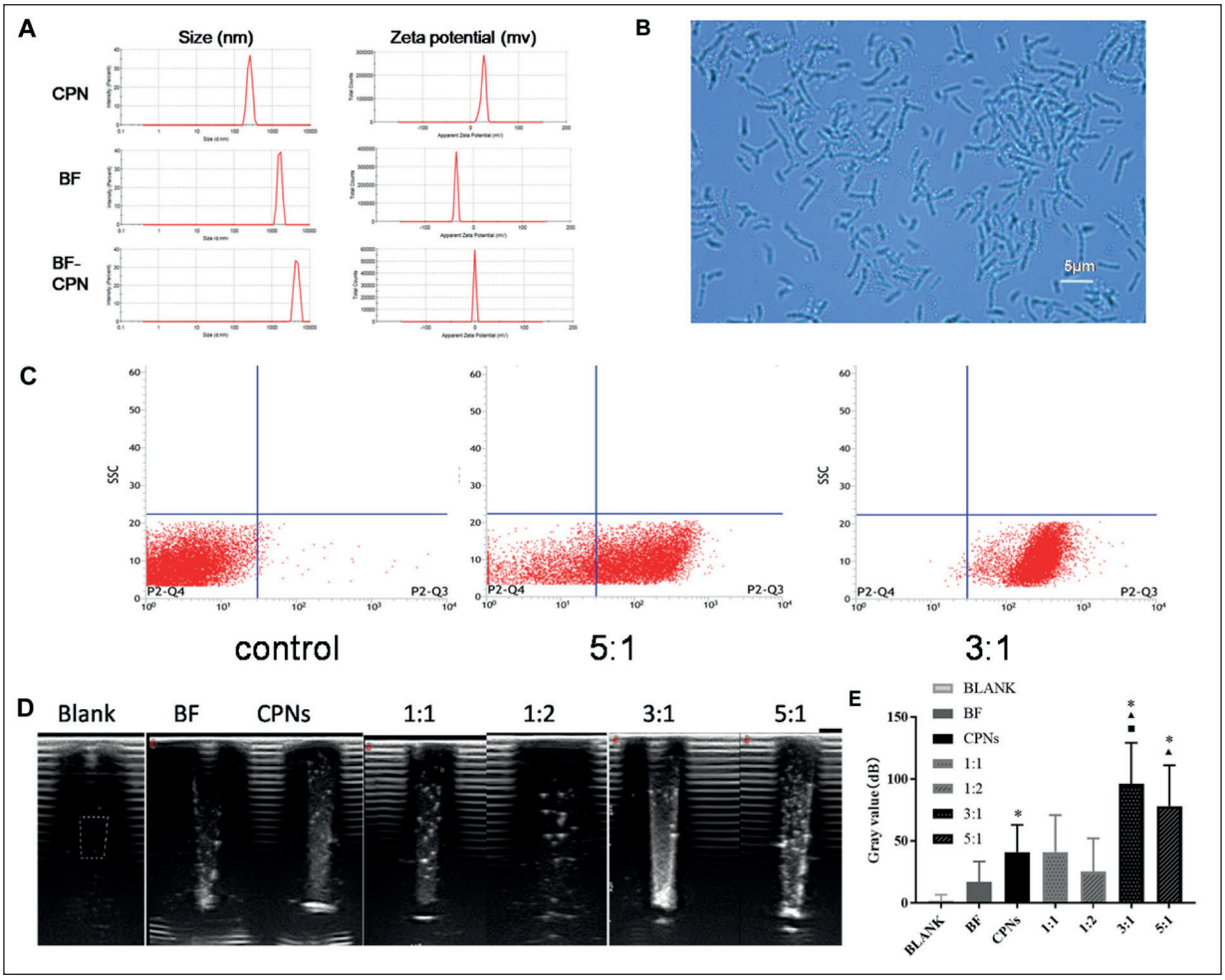

Figure 1. A, Particle size and zeta potential of CPNs, BF, and BF-CPNs, respectively. **B,** Racket-shaped, pole-shaped, Y-shaped, or V-shaped BF bonded to the surfaces of refractive NPs (magnification: 1000×). **C,** Flow cytometry disclosed that the BF-CPNs binding rate increased with CPNs proportion. **D,** Ultrasonic images of phantoms to which various proportions of BF-CPNs were added. Rectangular box indicates region of interest (ROI) based on gray value. **E,** Gray values for the sonograms of phantoms to which various proportions of BF-CPNs were added; *difference from blank control was statistically significant, $p<0.05$; ▲difference from BF was statistically significant, $p<0.05$; ▪difference from 2:1 mixture was statistically significant, $p<0.05$.

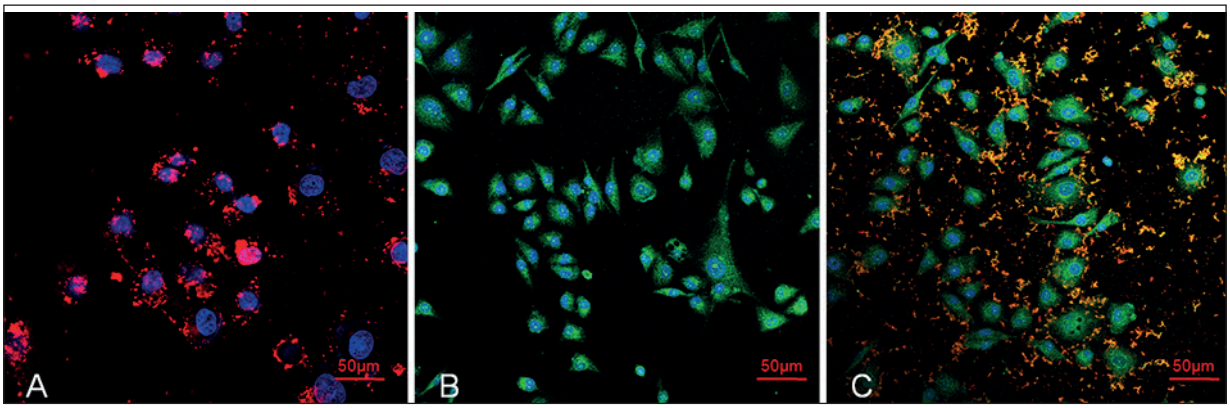

Figure 2. Co-incubation with breast cancer cells observed under confocal microscope. BF was labeled green by FITC. CPNs were labeled red by DiI. Breast cancer cell nuclei were labeled blue by DAPI (magnification: 800×). Pure NPs. **A,** CPNs surrounded the breast cancer cells. **B,** with no CPNs adhered to the cells. **C,** NPs-covered BF adhered to the cells and the overlapping staining was brown.

added to the breast cancer cells, large amounts of bacteria covered with NPs adhered to the cells. Almost no uncombined NPs surrounded the cells (Figure 2C)

Observation of Intratumoral BF-CPNs Injection and Stability In Vivo

The 2D and contrast-enhanced sonograms of each group at various time points were illustrated in Figure 3. No evident enhancement was noted for the BF and PBS groups at any time point. In the CPNs group, weak localized spotty echo enhancement was observed in 2D mode immediately after injection. However, there was no evident change in contrast mode. At 30 min, the local echo was enhanced and enlarged in 2D mode, spotty enhancement appeared in contrast mode, and the echo decreased. No image enhancement was observed in contrast mode after 12 h or in either mode after 24 h. In the experimental groups, the BF-CPNs complex was locally injected under ultrasound guidance. The incident path of the needle was detected in real-time in both the contrast and 2D modes. The injection area showed patchy enhancement immediately after the needle was retracted (Figure 4). Contrast signals were visible in the injection area at all time points in both the 2D and contrast modes. The echo in BF-CPNs2 was stronger than that for BF-CPNs1as the former was more concentrated than the latter. The echoes of the contrast agent decreased slightly and diffused after 48 h. The average local gray values of the 2D ultrasound images for each group at various time points were listed in Table I. The average gray values of BF-CPNs1 and BF-CPNs2 at various time points were significantly higher for the experimental group than the control and blank groups. The gray value for the CPNs group gradually peaked at 30 min-12 h, whereas that of the BF group reached a maximum

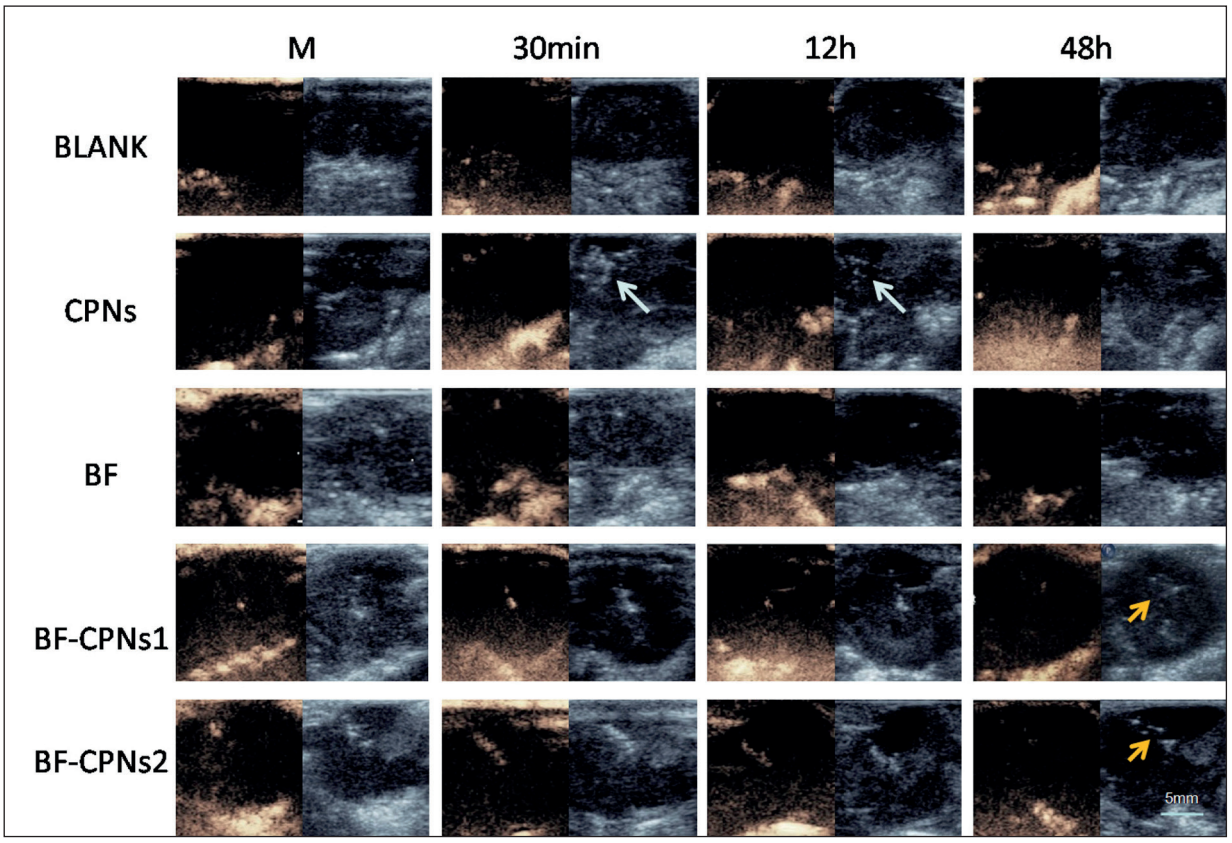

Figure 3. Contrast (*left*) and two-dimensional *(right*) ultrasound images of the injection areas at various time points. No clear imaging was detected for the blank (BLANK) and BF groups at any time point. There was light imaging in the CPNs group in 2D mode immediately after injection. Grayscale increased with dispersion (*white arrow*) within 30 min followed by markedly weakened imaging. There was no image in the contrast mode at 12 h. The BF-CPNs group showed enhanced images in contrast mode at all time points. The gray level increased with concentration of contrast agent then slightly decreased and dispersed by 48 h (*yellow arrow*).

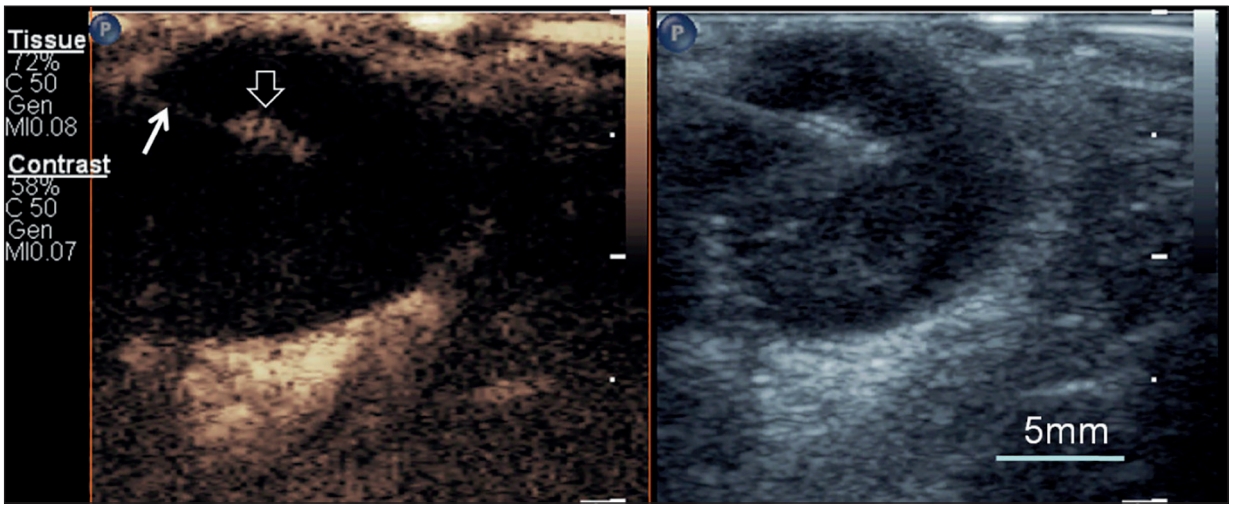

Figure 4. In contrast *(left)* and 2D (*right*) ultrasound modes, strong echo contrast was detected by real-time monitoring when BF-CPNs were locally injected under ultrasound guidance. Echo intensity = 109 dB in 2D mode. Injection needle (*thin arrow*). BF-CPNs (*thick arrow*).

during the period of 0 h-90 min. For both groups, the gray values substantially decreased thereafter.

The fluorescence assay *in vivo* showed that local fluorescence in the tumors of the CPNs and BF-CPNs groups increased after injection. Local tumor fluorescence in the CPNs group markedly decreased after 48 h while that for the BF-CPNs group remained significantly higher than that of the CPNs group (Figure 5). No evident fluorescence was detected in the other tissues or organs of nude mice.

Intratumoral BF-CPNs Injection Enhanced the Effect of HIFU Treatment

Ultrasonography was used during HIFU treatment to observe changes in local gray value and the areas of those changes (Figure 6A). After HIFU irradiation, coagulation necrosis was generally and histologically observed. It appeared as ovals or droplets with grayish-white medullae and grayish-red hemorrhagic foci (Figure 6B). There were significant differences in these parameters between the blank and the CPNs, BF-CPNs1, and BF-CPNs2 groups and between the BF-CPNs2 and CPNs groups (Figure 6C). The necrosis boundary was clear in the PBS and BF-CPNs groups. The BF-CPNs group presented with a relatively clearer boundary and broader ablation area than those of the control and PBS groups. The volume of ablative necrosis increased with BF-CPNs concentration (Figure 6C). After HIFU treatment, the centers of the ablation areas were completely stained red by H&E. In the experimental groups, cellular karyopyknosis and fragmentation were observed at the edges of the ablation areas. They formed a clear boundary between the ablation and non-ablation zones. The cells in certain normal tumor areas near the necrosis area expanded into empty vacuoles with large intercellular spaces (Figure 7A and

Table I. Average local gray value (dB) in 2D mode in each group; n = 6.

	1 min	10 min	30 min	1 h	90 min	12 h	24 h	48 h
Blank	18 ± 20.6	19 ± 3.1	15 ± 2.9	22 ± 2.0	21 ± 3.4	12 ± 2.2	14 ± 4.2	13 ± 3.7
BF	59 ± 70.2*	62 ± 4.7*	59 ± 5.2*	52 ± 4.4*	53 ± 5.1*	25 ± 3.9*	15 ± 3.6	20 ± 4.3*
CPNs	20 ± 30.3#	25 ± 2.3*#	58 ± 4.7*#	65 ± 4.1*#	72 ± 7.5*#	64 ± 5.8*#	27 ± 4.2*#	24 ± 3.1*
BF-CPNs-1&	96 ± 60.2	101 ± 7.3	97 ± 8.4	86 ± 7.2	88 ± 5.7	84 ± 4.6	77 ± 5.3	67 ± 4.8
BF-CPNs-2&	106 ± 5.9	109 ± 8.2	102 ± 6.4	98 ± 7.8	100 ± 7.5	94 ± 6.3	90 ± 5.0	79 ± 4.7

*Statistically significant difference from blank ($p<0.05$); #Statistically significant difference from BF ($p<0.05$); &Statistically significantly different average gray values of BF-CPNs-1 and BF-CPNs-2 from BLANK, BF, and CPNs at each time point ($p<0.05$).

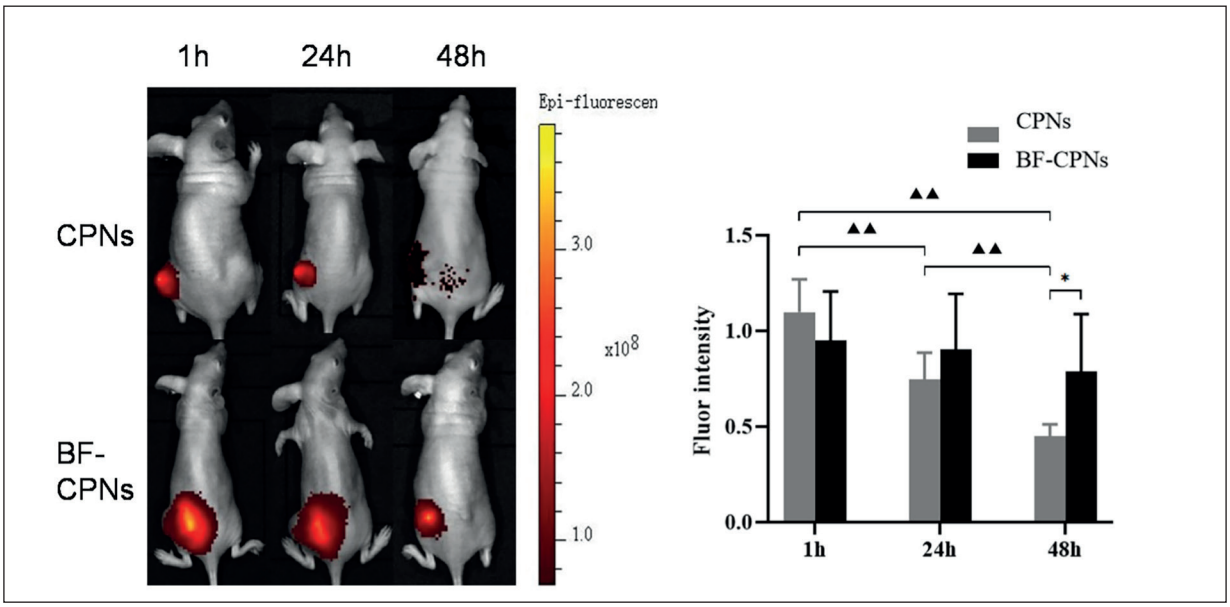

Figure 5. *In vivo* fluorescence imaging showed that the local tumor fluorescence intensity in the control group gradually decreased with time (▲$p<0.05$; ▲▲$p<0.01$). In contrast, there was no evident decrease in local tumor fluorescence intensity for the experimental group. The difference in local tumor fluorescence intensity between both groups was statistically significant by 48 h (*$p<0.05$). There was almost no fluorescence signal in the other tissues or organs of both groups at any time point.

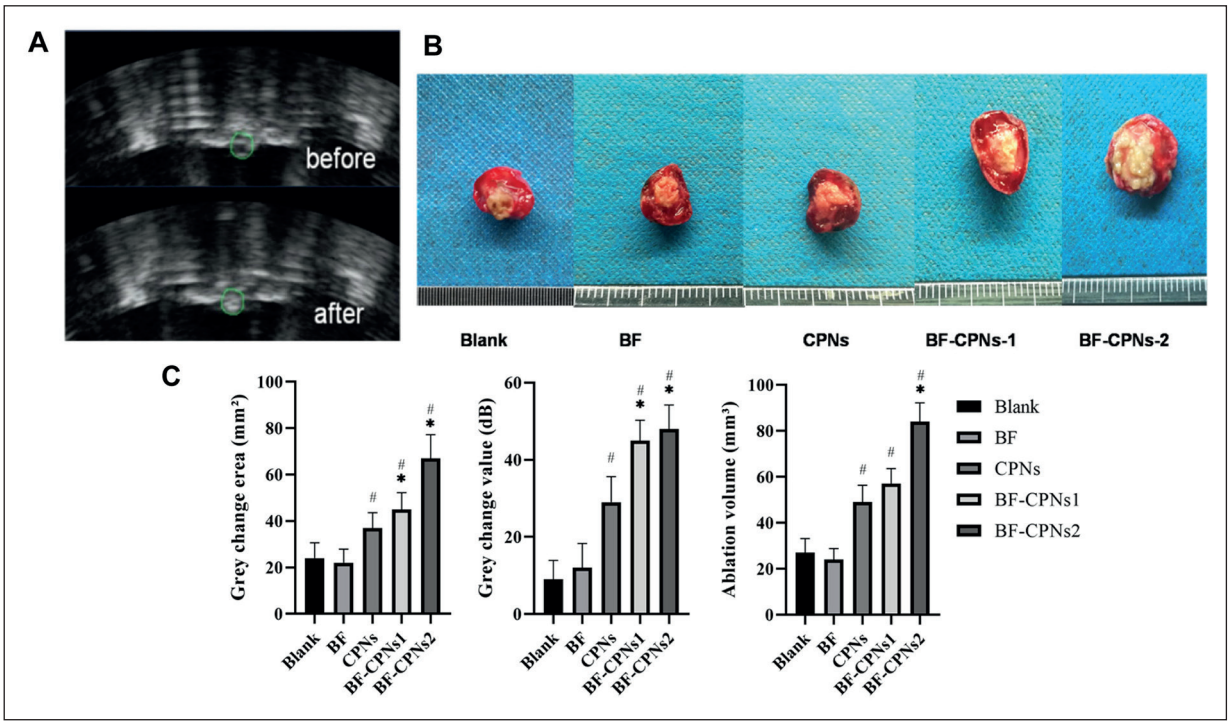

Figure 6. A, Change in the local gray value and the area of change before and after HIFU ablation combined with BF-CPNs injection. **B,** Gross section of tumor ablation (TTC staining) in each group. The white area is coagulation necrosis and the red area is unablated. There was a clear boundary in the experimental group. **C,** Changes in gray scale and the volume of gross necrosis were measured and compared among groups. #Significantly different from the blank and BF group ($p<0.05$). *Significantly different from the CPNs group ($p<0.05$). ▲Significantly different from the BF- CPNs-1 group ($p<0.05$).

7B). In the CPNs group, a wide thermal necrosis zone at the edge of the ablation zone was observed. The cells became misshapen as a result of karyopyknosis and fragmentation. Island-like residual areas were also seen in Figure 7C. Gram staining of the experimental groups disclosed numerous blue-stained (Gram-positive) regions of focal aggregations of rod-shaped bacteria in the tumor area. The blue staining in the ablation area consisted of bacterial debris as the particles had different sizes and irregular dot-or strip-like shapes (Figure 7D and 7E). In the non-ablation area, the bacterial morphology was relatively intact (Figure 7F). Bacterial growth was observed only in the tumor homogenate of the BF and BF-CPNs groups at 72 h. No bacterial growth was detected in the blood or other tissue homogenates (Figure 7G).

Discussion

In our study, CPNs with the positive charge bound to BF with negative charge at a high rate. The BF surface area is much larger than that of CPNs. Thus, numerous nanoparticles can attach

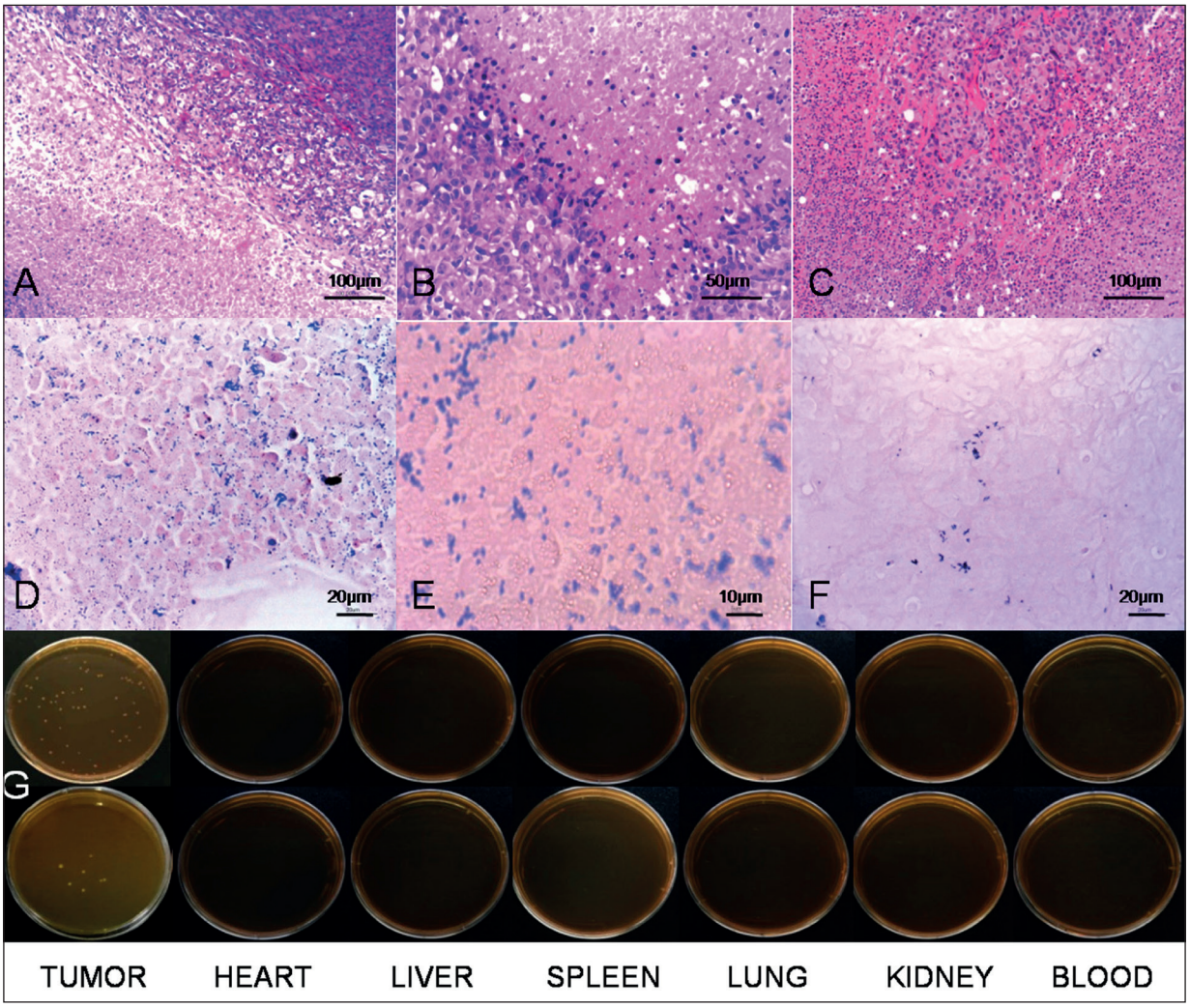

Figure 7. A, Boundaries among the coagulation necrosis area, the non-ablation area, and the edema zone were visible under × 100 light microscopy. A narrow band shaped karyopyknosis area (**B**) was observed at the edge of the coagulation necrosis zone. It was stained red in the center and the nuclei were absent (magnification: 200×). In the control group, there was a residual island-shaped non-ablation area (*arrow*) (**C**) and a wide karyopyknosis area at the edge of the necrosis area (magnification: 100×). Blue-stained BF in the necrosis area (magnification: 400×). **D**, BF fragments in the necrosis region (magnification: 1000×). **E**, Morphology of the BF in the non-ablation zone was intact (**F**, magnification: 400×). Growth of BF colonies (**G**, dilution factor = 10-4) was observed in the homogenized anaerobic cultures of the BF (upper) and BF-CPNs2 (*lower*) groups after 72 h.

to a single bacterium. This process is more effective than biotin-avidin or specific antibody binding, and it can result in substantial particle accumulation. Therefore, this synergistic agent can be used for *in vivo* and *in vitro* ultrasonic tracking. The properties and binding rates of various liposome-bifidobacterium complexes were investigated to determine the optimum binding ratio. The best echo contrast was obtained under 2D ultrasonography and it facilitated local injection and irradiation under ultrasound guidance. Image enhancement of BF-CPNs under ultrasonic exploration might be explained by a large number of nanoparticles enveloping the bacterial surfaces. This reaction creates acoustic impedance interfaces between the bacteria and the surrounding liquid. The net particle sizes of the nanoparticle-BF complex are comparable to those of micron-scale ultrasound contrast agents which scatter very effectively in diagnostic ultrasound. We further observed the interactions between BF-CNPs and tumor cells *in vitro*. Confocal microscopy showed that CPNs could promote adhesion between BF and tumor cells by functioning as a "two-sided glue". Adhesion is essential to the interaction between bacteria and host cells[24]. For this reason, nanoparticles may play this role after entering the body so as to enhance the aggregation of BF-CNPs complex in tumor.

Electrostatic adsorption-induced binding is simple and effective but its stability and durability still need a verification. In the present study, sustained levels of synergistic agents were detected in localized areas by ultrasonography and fluorescence *in vivo*. A similar phenomenon was observed in the tumor using intravenous CPNs and bifidobacterial in another study of our team[25]. Nanoparticles bounding to BF have long retention time because nanoparticles accumulating in response to bifidobacterial adhesion will not disperse into the interstitial space. Moreover, continuous bifidobacteria growth increases the local negative charge and tightens binding between BF and CPNs. In addition, covering specific antibodies on bacterial surfaces with cations may protect the nanoparticle complex from being captured and eliminated by the reticular system in the tumor area.

In the present study, intratumoral BF-CPNs injection was observed in animal models by ultrasound guidance. The local acoustic impedance differed markedly from that of the surrounding area after intratumoral injection. It formed a strong contrast on the sonogram with gray values $\geq$ 100 B. Furthermore, the contrast increased with the concentration of the mixture being injected. Forty-eight hours after injection, the agent could still be traced on the sonogram. This phenomenon has a profound impact on HIFU treatment under ultrasound guidance. It could be used for precise pre-treatment mapping of the synergistic area. Targeted ablation at the injection site of the synergistic agent could increase its therapeutic effect and reduce the risk of excessive ablation as the high echo in the ablation zone vanished after the microbubbles broke.

PFH was the core of the cationic nanoparticles. These were relatively stable, had a boiling point of 56°C, and were able to pass into the gas phase under ultrasound and thermal radiation. Previous studies[13,26-28] showed that synergists such as PFH emulsion and lipid- or polymer-encapsulated PFH enhanced HIFU treatment. In the present work, bifidobacteria were more effective than pure nanoparticles injection in promoting nanoparticles accumulation and enhancing HIFU treatment. The former resulted in complete coagulation necrosis and a clear boundary between the normal tissue and the ablation area. In contrast, pure nanoparticles injection may result in rapid dispersion, diffuse energy deposition, low dispersed nanoparticles concentrations, incomplete ablation, relatively wide thermal necrosis zones, and island-shaped residual lesions that could recur after HIFU treatment.

The biosafety of orally and intravenously administered bifidobacterium has been previously established[29-31]. In our study, bifidobacterium was administered by local intratumoral injection which has the advantages of strong targeting, low effective doses, and minimal impact on the whole body. However, synergistic agents will inevitably leak along the needle path into the surrounding normal tissues and are quickly absorbed by them. No bifidobacteria were found in the blood or solid organs. It was metabolized and scarcely affected the surrounding normal tissues. Moreover, no wound infection or death occurred in the nude mice during the experiment. Injections must be applied slowly. It is preferable to pause momentarily before withdrawing the needle to minimize leakage of the synergistic agent.

Local BF-CPNs injection based on the synergy between phase-change liquid fluorocarbon and bifidobacterial bio targeting and safety could enhance HIFU treatment efficacy under real-time ultrasonography. The BF-CPNs complex as a synergistic agent at the clinical trial level should

be verified. In future research, we will explore the correlations between injection dosage and synergistic effect, and we will try our best to improve the synergistic strategy and the assessment of ultrasound-based ablation efficacy.

Conclusions

BF and CPNs bind *via* electrostatic absorption. BF-CPNs can enhance accumulation and retention in tumors and are traceable by ultrasound. BF-CPNs can serve as a synergistic agent for HIFU treatment.

Conflict of Interest

The Authors declare that they have no conflict of interests.

Acknowledgements

The authors are greatly thankful for the financial support being offered by the Chongqing Basic Science and Frontier Technology Research Project (No. cstc2017jcyjAX0432), and the Chongqing Postdoctoral Scientific Research Project (No. Xm2017084).

References

1) Jakobsson J, Wickerts L, Forsberg S, Ledin G. Transversus abdominal plane (TAP) block for postoperative pain management: a review. F1000Res 2015; 4: 1359.
2) Liu Y, Xiong W, Xu JM, Liu YX, Zhang J. Correlations between the expression of C-erB-2, CD34 and ER in breast cancer patients and the signs of conventional ultrasonography and ultrasound elastography. Eur Rev Med Pharmacol Sci 2018; 22: 5539-5545.
3) Bu R, Yin L, Yang H, Wang Q, Wu F, Zou JZ. Tissue ablation accelerated by peripheral scanning mode with high-intensity focused ultrasound: a study on isolated porcine liver perfusion. Ultrasound Med Biol 2013; 39: 1410-1419.
4) Jiao J, Wu F, Zou J, Li F, Liu F, Zhao X, Wang Q. [Effect of ablations by pulsed versus continuous high-intensity focused ultrasound on isolated perfused porcine liver]. Nan Fang Yi Ke Da Xue Xue Bao 2013; 33: 230-234.
5) He W, Wang W, Zhou P, Wang YX, Zhou P, Li RZ, Wang JS, Ahuja AT. Enhanced ablation of high intensity focused ultrasound with microbubbles: an experimental study on rabbit hepatic VX2 tumors. Cardiovasc Intervent Radiol 2011; 34: 1050-1057.
6) Lin Y, Lin L, Cheng M, Jin L, Du L, Han T, Xu L, Yu A, Qin P. Effect of acoustic parameters on the cavitation behavior of SonoVue microbubbles induced by pulsed ultrasound. Ultrason Sonochem 2017; 35: 176-184.
7) Isern J, Pessarrodona A, Rodriguez J, Vallejo E, Gimenez N, Cassado J, De Marco JA, Pedrerol A. Using microbubble sonographic contrast agent to enhance the effect of high intensity focused ultrasound for the treatment of uterine fibroids. Ultrason Sonochem 2015; 27: 688-693.
8) Stride EP, Coussios CC. Cavitation and contrast: the use of bubbles in ultrasound imaging and therapy. Proc Inst Mech Eng H 2010; 224: 171-191.
9) Peng S, Hu L, Chen W, Chen J, Yang C, Wang X, Zhang R, Wang Z, Zhang L. Intraprocedure contrast enhanced ultrasound: the value in assessing the effect of ultrasound-guided high intensity focused ultrasound ablation for uterine fibroids. Ultrasonics 2015; 58: 123-128.
10) Chen Y, Jiang J, Zeng Y, Tian X, Zhang M, Wu H, Zhou H. Effects of a microbubble ultrasound contrast agent on high-intensity focused ultrasound for uterine fibroids: a randomised controlled trial. Int J Hyperthermia 2018; 34: 1311-1315.
11) Rouviere O, Glas L, Girouin N, Mege-Lechevallier F, Gelet A, Dantony E, Rabilloud M, Chapelon JY, Lyonnet D. Prostate cancer ablation with transrectal high-intensity focused ultrasound: assessment of tissue destruction with contrast-enhanced US. Radiology 2011; 259: 583-591.
12) Phillips LC, Puett C, Sheeran PS, Wilson MG, Matsunaga TO, Dayton PA. Phase-shift perfluorocarbon agents enhance high intensity focused ultrasound thermal delivery with reduced near-field heating. J Acoust Soc Am 2013; 134: 1473-1482.
13) You Y, Wang Z, Ran H, Zheng Y, Wang D, Xu J, Wang Z, Chen Y, Li P. Nanoparticle-enhanced synergistic HIFU ablation and transarterial chemoembolization for efficient cancer therapy. Nanoscale 2016; 8: 4324-4339.
14) Yao Y, Yang K, Cao Y, Zhou X, Xu J, Liu J, Wang Q, Wang Z, Wang D. Comparison of the synergistic effect of lipid nanobubbles and SonoVue microbubbles for high intensity focused ultrasound thermal ablation of tumors. PeerJ 2016; 4: e1716.
15) Singh R, Husseini GA, Pitt WG. Phase transitions of nanoemulsions using ultrasound: experimental observations. Ultrason Sonochem 2012; 19: 1120-1125.
16) Kopechek JA, Zhang P, Burgess MT, Porter TM. Synthesis of phase-shift nanoemulsions with narrow size distributions for acoustic droplet vaporization and bubble-enhanced ultrasound-mediated ablation. J Vis Exp 2012: e4308.
17) Paul S, Russakow D, Rodgers T, Sarkar K, Cochran M, Wheatley MA. Determination of the interfacial rheological properties of a poly (DL-lactic acid)-encapsulated contrast agent using in vitro attenuation and scattering. Ultrasound Med Biol 2013; 39: 1277-1291.
18) Liu T, Zhang N, Wang Z, Wu M, Chen Y, Ma M, Chen H, Shi J. Endogenous catalytic generation of O2

bubbles for in situ ultrasound-guided high intensity focused ultrasound ablation. Acs Nano 2017; 11: 9093-9102.

19) Huang J, Xu JS, Xu RX. Heat-sensitive microbubbles for intraoperative assessment of cancer ablation margins. Biomaterials 2010; 31: 1278-1286.

20) Kimura NT, Taniguchi S, Aoki K, Baba T. Selective localization and growth of Bifidobacterium bifidum in mouse tumors following intravenous administration. Cancer Res 1980; 40: 2061-2068.

21) Wang L, Vuletic I, Deng D, Crielaard W, Xie Z, Zhou K, Zhang J, Sun H, Ren Q, Guo C. Bifidobacterium breve as a delivery vector of IL-24 gene therapy for head and neck squamous cell carcinoma in vivo. Gene Ther 2017; 24: 699-705.

22) Cummins J, Cronin M, van Pijkeren JP, Gahan CG, Tangney M. Bacterial systems for gene delivery to systemic tumors. Methods Mol Biol 2014; 1141: 201-209.

23) Hasik MJ, Kim DH, Howle LE, Needham D, Prush DP. Evaluation of synthetic phospholipid ultrasound contrast agents. Ultrasonics 2002; 40: 973-982.

24) Westermann C, Gleinser M, Corr SC, Riedel CU. A critical evaluation of bifidobacterial adhesion to the host tissue. Front Microbiol 2016; 7: 1220.

25) Gao X, Zou W, Jiang B, Xu D, Luo Y, Xiong J, Yan S, Wang Y, Tang Y, Chen C, Li H, Qiao H, Wang Q, Zou J. Experimental study of retention on the combination of bifidobacterium with high-intensity focused ultrasound (HIFU) synergistic substance in tumor tissues. Sci Rep 2019; 9: 6423.

26) He K, Ran H, Su Z, Wang Z, Li M, Hao L. Perfluorohexane-encapsulated fullerene nanospheres for dual-modality US/CT imaging and synergistic high-intensity focused ultrasound ablation. Int J Nanomedicine 2019; 14: 519-529.

27) Cao Y, Chen Y, Yu T, Guo Y, Liu F, Yao Y, Li P, Wang D, Wang Z, Chen Y, Ran H. Drug release from phase-changeable nanodroplets triggered by low-intensity focused ultrasound. Theranostics 2018; 8: 1327-1339.

28) Zhao LY, Zou JZ, Chen ZG, Liu S, Jiao J, Wu F. Acoustic cavitation enhances focused ultrasound ablation with phase-shift inorganic perfluorohexane nanoemulsions: an in vitro study using a clinical device. Biomed Res Int 2016; 2016: 7936902.

29) Zhou H, He Z, Wang C, Xie T, Liu L, Liu C, Song F, Ma Y. Intravenous administration is an effective and safe route for cancer gene therapy using the bifidobacterium-mediated recombinant HSV-1 thymidine kinase and ganciclovir. Int J Mol Sci 2016; 17: 891.

30) Cronin M, Morrissey D, Rajendran S, El MS, van Sinderen D, O'Sullivan GC, Tangney M. Orally administered bifidobacteria as vehicles for delivery of agents to systemic tumors. Mol Ther 2010; 18: 1397-1407.

31) Tangney M. Gene therapy for cancer: dairy bacteria as delivery vectors. Discov Med 2010; 10: 195-200.